Unsupervised Change Detection for Hyperspectral Images

Michael Frank[1] and Mort Canty[2]

1. Introduction

Change detection is a central task in the field of remote sensing. Detection of anthropogenic or natural impacts on landcover is essential for many environmental studies. On the regional to global scale, only multitemporal remote sensing is capable of monitoring landcover changes caused by short-term phenomena such as fire hazards and seasonal vegetation change, or long-term phenomena such as urban development and desertification in a practical way. A variety of change detection techniques has been developed for multispectral satellite and airborne imagery, including arithmetic operations, methods of principle component analysis as well as post-classification comparison and multitemporal classification [Singh, 1989], [Roberts et al., 1998a], [Yuan et al., 1998]. Spectral change detection techniques rely on the principle that a difference exists in the spectral response of a pixel on two dates if the biophysical material within the instantaneous field of view (IFOV) has changed between these dates [Jensen, 1996]. Hyperspectral change detection has many advantages over multispectral data in detecting and discriminating surface properties because it provides a continuous spectrum across a range in wavelengths [Green et al., 1998]. Nevertheless, only few attempts have been made for change detection based on hyperspectral images [Wiemker et al., 1997]. Until recently, the main limiting factor on the employment of hyperspectral sensors in change detection studies has been inadequate multitemporal coverage [Garcia and Ustin, 2001]. But with the launch of the hyperspectral sensor Hyperion [EO1, 2000] and the growing number of hyperspectral airborne sensors, more of these images may be available soon, and with them a greater need for hyperspectral change detection methods. Past investigations mainly focused on the use of hyperspectral change detection for vegetation. Garcia (2001) [Garcia and Ustin, 2001] and Roberts (1999) [Roberts et al., 1997] use spectral mixture analysis to identify changes between soil, green vegetation (GV) and non-photosynthetic vegetation (NPV). But this involves time-consuming pre-processing and endmember selection to extract the amount and kind of changes depending on the selected classes. Other researchers used vegetation indices for change purposes [Chen et al., 1998], [Gamon and Qiu, 1999]. But all of these methods only considered specific changes. None of these methods accounts for general purpose monitoring, which is often needed to interpret the different changes in a global context. For example, changes in vegetation may often be due to anthropogenic influences. However, as multitemporal hyperspectral coverage increases even in those areas where no or little ground truth data is available the need for robust unsupervised change detection methods will be more evident than before.

The purpose of this study is to detect seasonal vegetation dynamics in the Santa Monica Mountains using an unsupervised hyperspectral change detection approach. Seasonal vegetation dynamics in arid and semi-arid areas are largely regulated by the availability of water. But climatic shifts and anthropogenic influences may also have a major impact on seasonal fluctuations. Therefore it is important to understand how these properties interact to predict long-term environmental consequences of climate and land use changes on ecosystem function and sustainability [Ustin et al., 1998]. However, detecting vegetation dynamics in the absence of land cover change is more challenging then standard land cover analyses because of the subtle community response [Garcia and Ustin, 2001]. Therefore we investigate the usefulness of a relatively new unsupervised change detection procedure for hyperspectral images. The so-called multivariate alteration detection (MAD) technique proposed by Nielsen and Conradsen (1998) [Nielsen et al., 1998]. In past studies this method has been successfully applied to multispectral images [Canty and Niemeyer, 2002], [Niemeyer et al., 1999], [Nielsen, 1996]. Here it was used to highlight seasonal changes in bitemporal Airborne Visible/ Infrared Imaging Spectrometer (AVIRIS) images from the Santa Monica Mountains (California). We applied the algorithm to selected bands as well as to all bands to test the usefulness of this method. The MAD bands were then examined to identify the quantity and the quality of changes. The results were compared with a derivative-based green vegetation index (DGVI) proposed by Chen and Elvidge (1998) [Chen et al., 1998] and a spectral mixture analysis (SMA) [Ustin et al., 1993] to provide a basis for comparison with other studies.

[1] ***Geographisches Institut der Rheinischen Friedrich-Wilhelms Universität, Bonn, Germany*** **(uzs5or@uni-bonn.de)**
[2] ***Forschungszentrum Jülich GmbH, Germany*** **(m.canty@fz-juelich.de)**

2. Methods

2.1 Study Site

The study site was located in the Santa Monica Mountains (California, USA). The range extends 70 km westward from the City of Los Angeles to Ventura, along the Pacific coast. Elevation ranges from sea level to about 900 m. This region is characterized by a Mediterranean climate, having cool, wet winters and hot, dry summers. The mean annual precipitation is 600 mm per year mainly falling between December and April. Temperatures exceed 35^{o}C in the summer but seldom drop below 10^{o}C in the winter. The rough, discontinuous, mountainous terrain is mostly dominated by chaparral vegetation communities, including drought-senescent "soft" chaparral (coastal sage scrub) and evergreen "hard" chaparral [Barbour and Major, 1990]. Hard chaparral (dominated by *Ceanothus spp.* and *Adenostoma fasciculatum*) is mainly distributed at higher elevations on the interior side of the range. Soft chaparral (dominated by *Salvia* and *Eriogonum spp.* and *Artesemia californica*) is more common in the coastal area at lower elevation but does also occur in isolated patches at higher elevation on outcrops of shallow or fine textured soils [Holland and Keil, 1967]. However, vegetation patterns are complicated by the complex spatial distribution of chaparral species due to steep topographic gradients, variable fire histories, a complex landownership and different soil types [Roberts et al., 1998b].

2.2 AVIRIS Data

AVIRIS collects spectra in the wavelength range from 390 to 2500 nm in 224 bands with a nominal spectral response of 10 nm [Green et al., 1998]. The sensor is mounted on an ER-2 aircraft, flying at an elevation of approximately 20 km resulting in an IFOV of 20 m on the ground. A typical AVIRIS scene consists of 614 * 512 pixel (~ 11 km * 8 km).

Bitemporal AVIRIS data sets were acquired over the Santa Monica Mountains on 23 October 1996 and on 7 April 1997. The data presented here were obtained from flight-lines *f970407t01p02*, *run 06, scene 04* and *f961023t01p02 run 04*, *scene 05 and 06*, centered over Point Dume, California (34 ^{o}5`N, 118 $^{o}$40`W). The images from 1996 were acquired 3 days after the Calabasas fire at the end of the dry Mediterranean summer, whereas the 1997 image represents a period of spring growth.

2.3 Preprocessing

Atmospheric correction was done using the MODTRAN 3 radiative transfer code to process the AVIRIS radiance data to reflectance. To retrieve apparent surface reflectance a method proposed by Green et al. [Green et al., 1993], Roberts et al. [Roberts et al., 1997] was applied on the MODTRAN corrected images. This model accounts for a spatially variable atmosphere, such as found over mountainous terrain. The images from fall 1996 were then mosaicked to cover the scene from spring 1997.

A tedious task associated with change detection is the registration of the images involved, in particular the setting of ground control points (GCPs). Registration errors will tend to reduce the accuracy of any digital change detection effort. It is essential that registration accuracies should be on the order of half a pixel or less, to avoid false change signals as much as possible. A typical problem of hyperspectral imagery recorded with airborne line scanners is that normal registration techniques like polynominal fitting yield accuracies of some pixels at best. This displacement is caused by the varying flight tracks of the aircraft (in contrast to satellites) and the usually large swath angles of airborne scanners which allow for oblique viewing angles. Therefore, imagery from airborne scanners in general requires locally adaptive transformation functions [Wiemker et al., 1997]. For the image-to-image registration, the scene from 1997 was used as base image and a thin plate spline model (TPS) was applied to compute the warping transformation [Geomatics, 1997]. This model computes, in addition to a global transformation, local interpolation functions between the GCPs. To ensure an accurate change detection registration, 400 GCPs were manually digitized. 150 GCPs were selected as check points to compute the root mean square error (RMS) of the transformation. The overall accuracy of the registration was about 0.41 pixels.

In order to preserve the spectral characteristics of the data as much as possible resampling was done using the nearest neighbor method. For further processing, 165 AVIRIS bands were selected and a sea mask was applied to the co-registered AVIRIS images.

2.4 Multivariate Alteration Detection (MAD)

The MAD procedure is an application of a classical statistical transformation referred to as canonical correlation and will briefly be described here. In general, hyperspectral imagery for monitoring purposes is recorded

by multitemporal overflights over the same land area. We represent hyperspectral pixel intensities measured at two different times by random vectors X and Y:

$$X = \begin{pmatrix} X_1 \\ \vdots \\ X_N \end{pmatrix}, \qquad Y = \begin{pmatrix} Y_1 \\ \vdots \\ Y_N \end{pmatrix} \tag{1}$$

N being the number of spectral components, then we search for a linear transformation

$$u = a^T X = a_1 X_1 + \cdots a_N X_N, \tag{2}$$

$$v = b^T Y = b_1 Y_1 + \cdots b_N Y_N, \tag{3}$$

where the coefficients a_i and b_i $(i = 1... N)$ are as yet unspecified. In order to detect the changes between the two images, we calculate the difference $U – V$. As an advantage of this procedure all the information is combined into a single image, and one is free to choose the coefficients a_i and b_i in a suitable way. The MAD procedure determines these coefficients so that the positive correlation between U and V is minimised [Nielsen, 1994].

In fact, we search for a linear transformation such that the difference between the transformed vectors has maximum variance:

$$\mathrm{var}(u - v) = \mathrm{var}\left(a^T X - b^T Y\right) \rightarrow \text{Maximum} \tag{4}$$

subject to the constraint

$$\mathrm{var}(u) = \mathrm{var}(v) = 1 \tag{5}$$

Under these constraints we have:

$$\mathrm{var}(u - v) = \mathrm{var}(u) + \mathrm{var}(u) - 2\,\mathrm{cov}(u, v) = 2(1 - corr(u, v)). \tag{6}$$

Therefore, we seek vectors a und b, which minimizes the positive correlation $corr(u, v)$. Mathematically this involves the solution of a generalized eigenvalue problem [Anderson, 1984]. The MAD transformation is then described as:

$$\begin{pmatrix} X \\ Y \end{pmatrix} \rightarrow \cdots \begin{pmatrix} a_1^T - b_1^T \\ \vdots \\ a_N^T - b_N^T \end{pmatrix} \tag{7}$$

where a_i and b_i are the defining coefficients from a standard canonical correlation analysis. X and Y are vectors with mean zero.

As a result we obtain as many MAD bands as input channels, whereby the last MAD component has maximum spread in its pixel intensities and, ideally, maximum change information. The second-to-last component has maximum variance subject to the condition that the pixel intensities are statistically uncorrelated with those in the first component, etc. Figure 1 shows a scatterplot of MAD1 vs. MAD2 for two AVIRIS scenes. The components are seen to be uncorrelated and approximately Gaussian. Assuming that different kinds of changes will generally be

uncorrelated with one another, these changes will be distributed among different MAD components. Noise will be concentrated in lower order components [Canty et al., 2001].

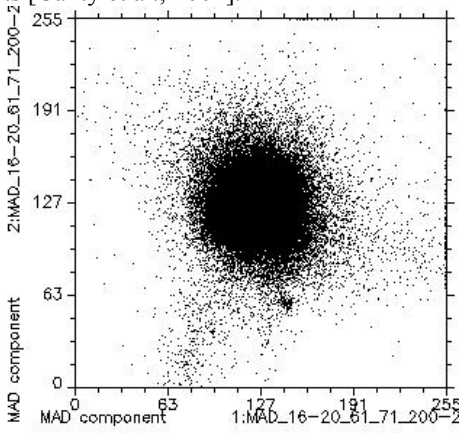

Figure 1: Scatterplot MAD1 vs. MAD2.

The MAD procedure is invariant to linear scaling. Therefore, it is insensitive to, for example, differences in gain and offset settings in a measuring device, and to the application of radiometric and atmospheric correction schemes that are linear in the digital numbers (DN) of each image band [Nielsen, 1999]. The MAD method can also be applied on any spatial and/or spectral subset of the full data set to focus the analysis in any desired manner. For specific applications, certain wavelength bands may be selected, whereby for general purpose monitoring, all spectral bands can be taken into account (see equation 2 and 3).

The resulting MADs can qualitatively be interpreted by

- ***visual interpretation***
- ***magnitude and direction of the changes***
- ***correlation with the original AVIRIS bands***

Furthermore the MAD method can be computed completely automatically because the calculation of the transformation is solely determined by the statistical properties (spectral dispersion matrices) of the original image data [Canty et al., 2001].

For cases where many spectral bands are to be used, pre-processing via the MNF (minimum noise fraction) transformation and/or post-processing by means of a MAF (minimum/maximum autocorrelation factor) transformation could be useful [Nielsen et al., 1998].

3. Results and Discussion

In unsupervised change detection studies, where little or no ground truth data are available, it is very useful to get a rough estimation of the expected changes. Besides visual interpretation this can be done by using some fundamental image statistics. Therefore the mean and the standard deviations of both images were computed for every band and compared with one another to provide insight into the type of process that may have produced the changes (Figure 2).

In Figure 2(b) the AVIRIS scene of October shows higher spectral variations in the NIR/SWIR. In addition, the mean signature of the AVIRIS scene of April (Figure 2(a)) shows a more pronounced red edge, chlorophyll and water absorption as well as lower mean values in the NIR and SWIR compared with the scene from October. On the basis of visual examination and due to the fact that both scenes are mainly covered with vegetation the signatures in the figure could be interpreted as a subsequent drying of the vegetation from April to October with an increasing amount of NPV and Soil at the expense of GV.

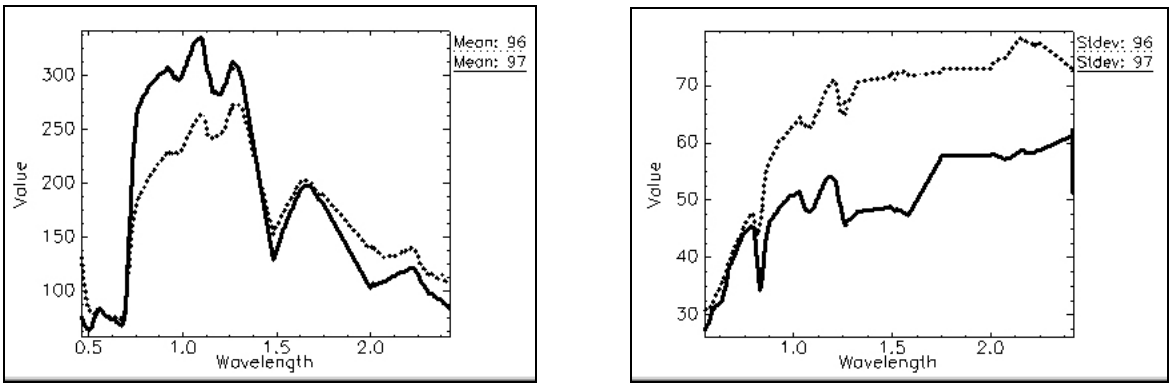

(a) mean **(b)** standard deviations

Figure 2: Mean **(a)** and standard deviations **(b)** from April 1997 (thick line) and October 1996 (dotted line) calculated over all AVIRIS bands.

The MAD method was applied to the co-registered images using:

(i) ***vegetation specific bands***

(ii) ***MNF bands***

(i) Wavelength regions from 673-702 nm (chlorophyll absorption), 770-818 nm (rededge shoulder), 1173-1211 nm (plant water absorption), 2088-2138 nm (ligno-cellulose absorption) and 2288-2338 nm (ligno- cellulose absorption) were selected as input channels for the MAD method in order to enhance these phenological changes as much as possible. The AVIRIS scene from April was selected as the base image in the MAD transformation. In order to detect the subtle vegetation dynamics we applied manual thresholding with 1.5 Standard deviations from the mean for the discrimination of change and no-change pixels. The MAD components are linearly stretched from mean minus and plus three standard deviations. The results of the MAD transformation (first 6 components) are shown in Figure 3. Maximum change areas are shown as white (positive changes) and black (negative changes) pixels. Gray areas indicate no change. Correlations between the change areas of the MADs and the original AVIRIS data (wavelength regions) are shown in Table 1.

Table 1: Correlation matrix of the MAD components with the original AVIRIS bands.

Date and wavelength region	**MAD 1**	**MAD 2**	**MAD 3**	**MAD 4**	**MAD 5**	**MAD 6**
April 7th (673-702 nm)	0.19	0.10	0.02	0.06	-0.08	0.00
April 7th (770-818 nm)	0.25	0.19	-0.07	0.09	-0.06	0.03
April 7th (1173-1211 nm)	0.15	-0.16	0.02	0.05	-0.09	-0.05
April 7th (2088-2138 nm)	0.16	-0.02	0.16	0.18	-0.00	-0.05
April 7th (2288-2338 nm)	0.11	-0.02	0.16	-0.19	0.02	-0.12
October 23rd (673-702 nm)	-0.11	0.10	-0.09	0.06	0.03	-0.04
October 23rd (770-818 nm)	-0.15	-0.21	-0.02	-0.08	0.04	-0.09
October 23rd (1173-1211 nm)	-0.25	0.19	-0.08	0.05	0.03	-0.07
October 23rd (2088-2138 nm)	-0.22	0.08	-0.28	0.16	0.08	0.01
October 23rd (2288-2338 nm)	-0.24	0.08	-0.22	0.28	0.09	-0.05

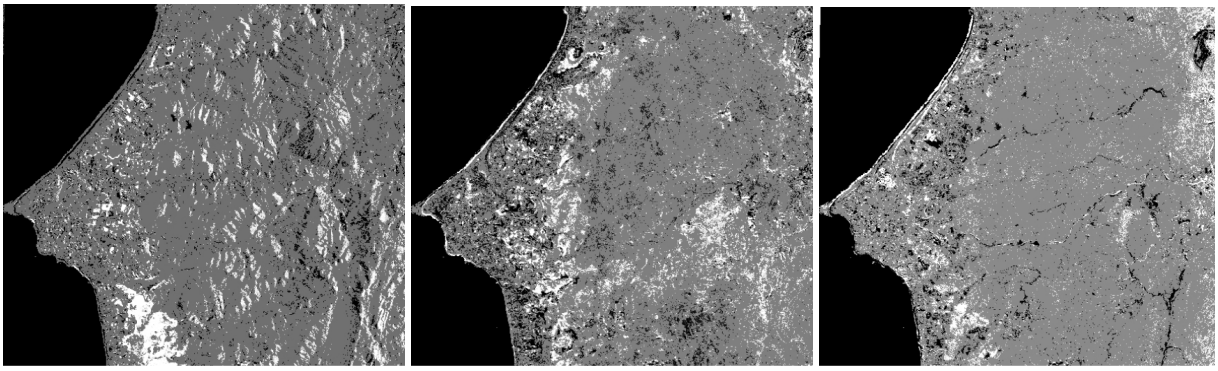

(a) MAD 1 **(b)** MAD 2 **(c)** MAD 3

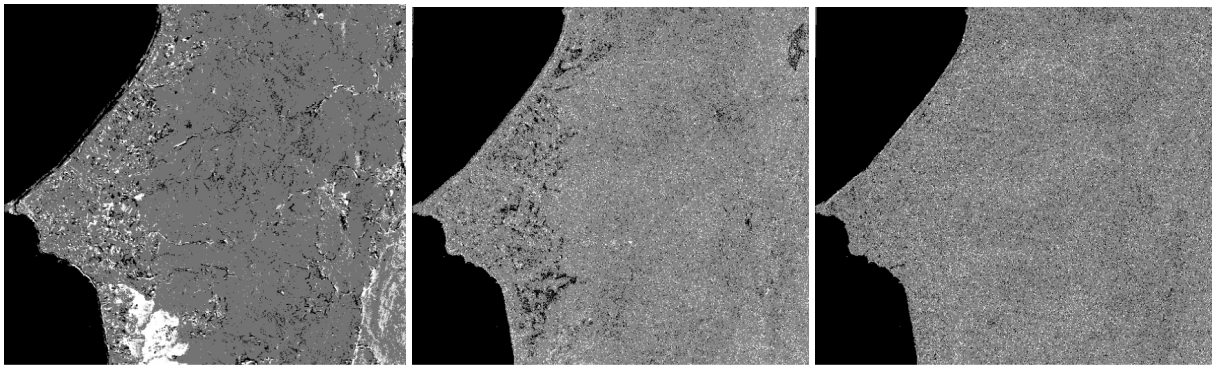

(d) MAD 4 **(e)** MAD 5 **(f)** MAD 6

Figure 3: MAD components 1 to 6 **(a-f)**.

As mentioned above, MAD1 shows the largest changes. The correlation of MAD1 shows a weighted mean of all channels with positive correlation in the October image and negative correlation in the April image. Therefore MAD1 is probably an indicator of shadow-induced changes. Actually, if we consider MAD1 (Figure 3(a)) [*] we can identify positive and negative changes mainly located in east-west valleys, which are strongly effected by intense shadowing. Positive changes at the Calabasas fire site (at the lower middle site of the image) are due to post-fire vegetation re-growth from October to April. In MAD2 we expect smaller changes that are furthermore uncorrelated to MAD1. Therefore more subtle changes, such as changes in phenology, are expected to occur in MAD2 and lower order MAD components. In fact MAD2 correlates with bands in the NIR and Red and could therefore be sensitive to changes in GV. Figure 3(b) shows high positive changes at the coastal region and in some isolated patches in the interior. These changes are consistent with the distribution of the soft chaparral communities. Soft chaparral is drought-deciduous and exhibits pronounced seasonal changes. Because seasonal vegetation dynamics in Mediterranean-climate ecosystems are mainly driven by the effect of water, most of the changes in the chaparral communities were basically due to loosing green leaves. Negative changes represent seasonal dynamics in hard chaparral communities. Most hard chaparral species are evergreen and undergo little seasonal senecense.

MAD3 and MAD4 have highest correlation in the SWIR regions and are presumably change indicators of NPV and/or soil. In general the change-enhanced data of MAD3 (Figure 3(c)) and MAD4 (Figure 3(d)) show small areas of changes in the soft chaparral areas. However, because of the larger changes at the Calabasas fire site, MAD4 seems to be more likely to represent changes in soil. Linear changes in MAD3 and MAD4 are probably due to poor registration of roads. MAD5 (Figure 3(e)) and MAD6 (Figure 3(f)) are uncorrelated with all bands in both years and show scanner noise.

Changes in the urbanized area apparent in all MAD components are probably due to registration errors, irrigation or seasonal planting of different flowers or plants. The golf course at the upper right shows high changes in some MAD components induced by irrigation and soil moisture. The changes at the coastline are caused by waves

[*] In this article all images are rotated 90 degrees clockwise.

and tides. Different changes at the Calabasas fire site best seen in (Figure 4(a)) are presumably due to the successive stages of post-fire vegetation re-growth.

In comparison to the SMA (not shown) we see a general agreement between the MAD components and the fraction images (GV, NPV, soil and shadow) of the SMA.

(ii) In order to concentrate and to visualize all spectral change information in one composite image the MAD transformation was performed based on a MNF transformation [Green et al., 1988] calculated from 165 AVIRIS bands. We used the first 10 MNF Bands describing 90% of the variance of the image data. Figure 4(a) shows the RGB image of MAD/MNF components two, three and four with the same decision threshold (MAD/MNF1 as an indicator of shadow induced changes was rejected).

To provide a basis for comparison with other methods a DGVI difference image (Figure 4(b)) with the same decision threshold as applied on the MAD transformation was computed [Chen et al., 1998]. In the MAD/MNF composite we can see more changes than in the DGVI difference image, especially in the housing estate areas, the Calabasas fire site and at the golf course.

In addition, a change probability based on a MAD transformation calculated from all 165 AVIRIS bands was performed. It was calculated using the sum of standardized, squared MADs [Canty et al., 2003] (see equation 8):

$$\sum_{i=1}^{N}\left(\frac{MAD_i}{\sigma MAD_i}\right)^2 \tag{8}$$

The resulting image (Figure 5) is approximately chi-square distributed with six degrees of freedom describing a change probability of 95%.

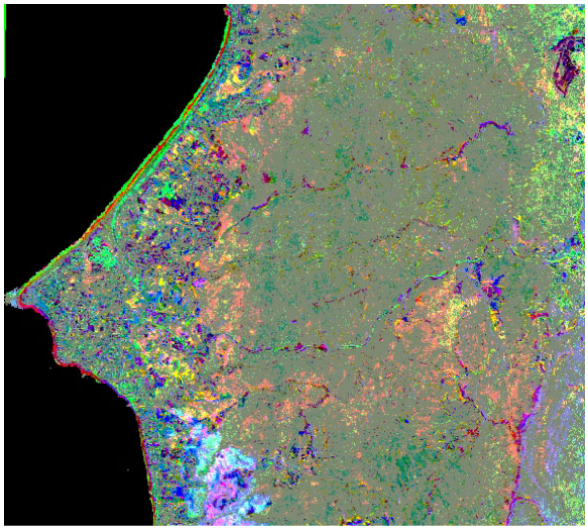

a) MAD/MNF RGB composite image with R=*MAD/MNF2,* G=*MAD/MNF3,* B=*MAD/MNF4*

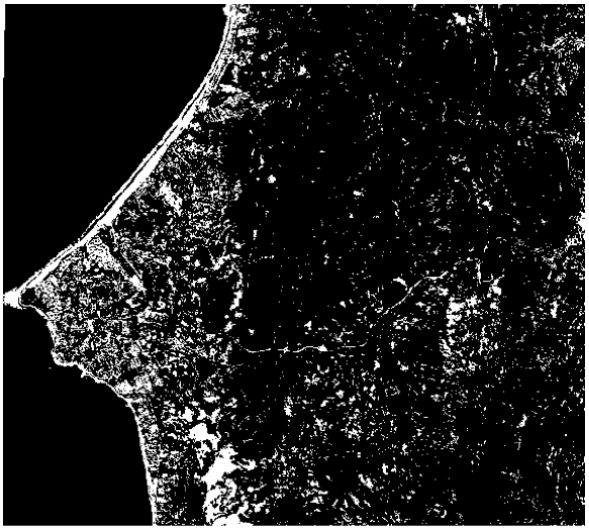

(b) DGVI change mask

Figure 4: Comparison between MAD/MNF and DGVI.

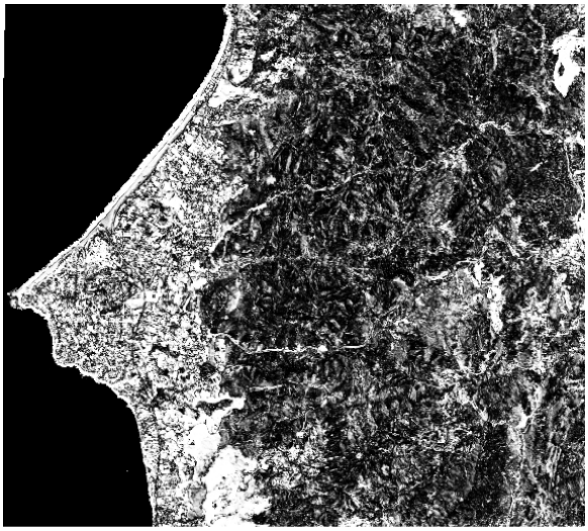

Figure 5: MAD change probability. White areas represent changes with a probability of 95%.

4. Conclusion

The applicability of the MAD method to hyperspectral, bitemporal, unsupervised change detection studies was demonstrated and an interpretation approach based on the correlation matrix was given. The MAD transformation was applied on bitemporal AVIRIS images of the Santa Monica Mountains to detect seasonal changes. The method was performed on selected bands, MNF bands as well as to all bands. The main changes observed are due to contrasting seasonal patterns of chaparral communities. Large change areas are located within soft chaparral communities and at the Calabasas fire site. The lowest changes occurred in areas covered with hard chaparral. In addition changes that can be related to registration errors, irrigation practices, shadow formation and other anthropogenic influences were also shown by the MAD method. As expected subtle vegetation changes occurred in the lower order MAD components whereas large changes like shadow formation are more apparent in the first MAD components.

We found the MAD transformation to be a good unsupervised change detection method for hyperspectral images. It can be applied on any spatial and/or spectral subset of the full data set and sorts different changes into different images. The MAD transformation is also comparable to other methods based upon DGVI or SMA. MAD tends to be robust against varying recording conditions at the time of the data acquisition and can be run completely automatically. But as for all change detection techniques a good registration accuracy is needed. On the other hand, interpretation of the MAD components is difficult when many spectral bands are used, so data reduction is sometimes necessary as a pre- and/or post-processing step. In general, the MAD transformation seems to be suitable for all kinds of change detection applications.

Acknowledgements

The Authors would like to thank Dar Roberts, Phil Dennison and Martin Herold from UCSB, Santa Barbara, for their provision of the atmospherically corrected images and for helpful suggestions. We also would like to thank Allan Nielsen (Technical University of Denmark, Lyngby) and Gunter Menz (University of Bonn) for helpful discussions.

References

[EO1, 2000]. Hyperion on EO-1. URL: *http://eo1. gsfc. nasa. gov*.

[Anderson, 1984] Anderson, T. W. (1984). An Introduction to Multivariate Statistical Analysis. New York. Wiley, New York, 2nd edition edition.

[Barbour and Major, 1990] Barbour, M. G. and Major, J. (1990). Terrestrial vegetation of California. Special publication No. 9. California Native Plant Society Press, University of California, Davis.

[Canty and Niemeyer, 2002] Canty, M. and Niemeyer, I. (2002). Analysis of digital satellite imagery. In Jasani, B. and Stein, G., editors, Commercial Satellite Imagery. A tactic in nuclear weapon deterrence, pages 67–78. Springer, Berlin Heidelberg.

[Canty et al., 2001] Canty, M., Niemeyer, I., Truong, B., et al. (2001). Change detection with multispectral satellite imagery: Application to nuclear verification. Proceedings of the International Symposium on Spectral Sensing Research, Quebec City. ISSSR.

[Canty et al., 2003] Canty, M., Nielsen, A. A., and Schmidt, M. (2003). Automatic radiometric normalization of multitemporal multispectral imagery. Remote Sensing of Environment, page in press.

[Chen et al., 1998] Chen, Z., Elvidge, C. D., and Groeneveld, D. P. (1998). Monitoring seasonal dynamics of arid land vegetation using AVIRIS data. Remote Sensing of Environment, 65(2): 255–266.

[Gamon and Qiu, 1999] Gamon, J. A. and Qiu, H. (1999). Ecological applications of remote sensing at multiple scales. In Pugnaire, F. I. and Valladares, F., editors, Handbook of functional plant ecology, chapter 23, pages 805–846. Marcel Dekker, New York.

[Garcia and Ustin, 2001] Garcia, M. and Ustin, S. L. (2001). Detection of interannual vegetation responses to climatic variability using AVIRIS data in a coastal savanna in California. IEEE Transactions on Geoscience and Remote Sensing, 39(7): 1480–1490.

[Geomatics, 1997] Geomatics, PCI. (1997). GCP Works User Manual. PCI Geomatics.

[Green et al., 1988] Green, A. A. et al. (1988). A transformation for ordering multispectral data in terms of image quality with implications for noise removal. IEEE Transactions on Geoscience and Remote Sensing, 26: 65–74.

[Green et al., 1993] Green, R. O., Conel, J. E., and Roberts, D. A. (1993). Estimation of aerosol optical depth and additional atmospheric parameters for the calculation of apparent reflectance from radiance measured by the airborne visible/ infrared imaging spectrometer (AVIRIS). Summaries of the Fourth JPL Geoscience Airborne Workshop, Wahington D. C., pages 73–76.

[Green et al., 1998] Green, R. O. et al. (1998). Imaging spectroscopy and the airborne visible/ infrared imaging spectrometer (AVIRIS). Remote Sensing of Environment, 65: 227–248.

[Holland and Keil, 1967] Holland, V. L. and Keil, D. J. (1967). California vegetation. California Polytechnic State University, San Luis Obispo.

[Jensen, 1996] Jensen, J. R. (1996). Introductory Digital Image Processing. Prentice Hall, New Jersey.

[Nielsen, 1994] Nielsen, A. A. (1994). Analysis of regularly and irregularly sampled spatial, multivariate, and multi-temporal data. PhD thesis, Informatics and Mathematical Modelling, Technical University of Denmark, Richard Petersens Plads, Building 321, DK-2800 Kongens Lyngby, Denmark.

[Nielsen, 1996] Nielsen, A. A. (1996). Change detection in multi-spectral, bi-temporal spatial data using orthogonal transformations. 8th Australasian Remote Sensing Conference, Canberra, Australia.

[Nielsen, 1999] Nielsen, A. A. (1999). Multi-channel remote sensing data and orthogonal transformations for change detection. In Kanellopoulos, I., Wilkinson, G., and Moons, T., editors, Machine Vision and Advanced Image Processing in Remote Sensing, pages 37–48. Springer, Berlin.

[Nielsen et al., 1998] Nielsen, A. A., Conradsen, K., and Simpson, J. J. (1998). Multivariate alteration detection (MAD) and MAF postprocessing in multispectral, bitemporal image data: New approaches to change detection studies. Remote Sensing of Environment, 64(1): 1–19.

[Niemeyer et al., 1999] Niemeyer, I., Canty, M., and Klaus, D. (1999). Unsupervised change detection techniques using multispectral satellite images. IEEE International Geoscience and Remote Sensing Symposium, Hamburg. IGARSS.

[Roberts et al., 1998a] Roberts, D. A., Batista, G., Pereira, J. L., et al. (1998a). Change identification using multitemporal spectral mixture analysis: Applications in eastern Amazonia. In Elvidge, C. D. and Lunetta, R., editors, Remote Sensing Change Detection: Environmental Monitoring Applications and Methods, chapter 9, pages 137–161. Ann Arbor Press.

[Roberts et al., 1998b] Roberts, D. A., Gardener, M., Church, R., et al. (1998b): Mapping chaparral in the Santa Monica Mountains using multiple endmember spectral mixture models. Remote Sensing of Environment, 65: 267–279.

[Roberts et al., 1997] Roberts, D. A., Green, R. O., and Adams, J. B. (1997). Temporal and spatial patterns in vegetation and atmospheric properties from AVIRIS. Remote Sensing of Environment, 62: 223–240.

[Singh, 1989] Singh, A. (1989). Digital change-detection techniques using remotly-sensed data. International Journal of Remote Sensing, 10(6): 989–1003.

[Ustin et al., 1998] Ustin, S. L., Roberts, D., and Hart, Q. J. (1998). Seasonal vegetation patterns in a California coastal savanna derived from advanced visible/infrared imaging spectrometer AVIRIS data. In Elvidge, C. D. and Lunetta, R., editors, Remote Sensing Change Detection: Environmental Monitoring Applications and Methods, chapter 10, pages 163–176. Ann Arbor Press.

[Ustin et al., 1993] Ustin, S. L., Smith, M., and Adams, J. B. (1993). Remote sensing of ecological processes: a strategy for developing ecological models using spectral mixture analysis. In Ehlringer, J. and Fields, C., editors, Scaling Physiological Processes: Leaf to Globe, chapter 19, pages 339–357. Academic Press, San Diego, Kalifornien.

[Wiemker et al., 1997] Wiemker, R., Speck, A., Kulbach, D., et al. (1997). Unsupervised robust change detection on multispectral imagery using spectral and spatial features. Proceedings of the Third International Airborne Remote Sensing Conference and Exhibition, 1 (Copenhagen): 640–647.

[Yuan et al., 1998] Yuan, D., Elvidge, C., and Lunetta, R. (1998). Survey of multispectral methods for land cover change analysis. In Elvidge, C. D. and Lunetta, R., editors, Remote Sensing Change Detection: Environmental Monitoring Applications and Methods, chapter 2, pages 21–39. Ann Arbor Press.